On the Optimization of Cost Functions in Absolute Plate Motion Modeling

James Unwin and Steve Zhang

Abstract

In this paper, we investigate the optimization framework of optAPM, a leading code for absolute plate motion modeling. We address systematic errors present in these models, primarily resulting from inconsistencies and gaps in data. Through a comprehensive analysis of the three different constraints integral to optAPM's functionality, we identify several key concerns regarding model integrity. We introduce new cost functions for both hotspot trail misfit and net lithospheric rotation, grounded in objective statistical principles. Additionally, we facilitate the interpolation of hotspot trails, crucial geological markers for validating absolute plate motion over millions of years. By enhancing hotspot chain data, this study achieves a marked increase in the predictive accuracy and reliability of the optAPM outputs. The refined model significantly mitigates the propagation of errors, leading to more precise reconstructions of historical plate movements.

1 Introduction

The theory of continental drift presents Earth's surface as a composition of many tectonic plates, whose movement and deformation shape our planet over geological timescales. For decades, scientists have studied this phenomenon from a variety of perspectives. However, challenges persist due to discrepancies among datasets utilized in plate tectonic studies, often resulting from large spatial and temporal gaps in available data and human measurement errors. The plate tectonic system as a whole is extremely noisy, characterized by the constant subduction of oceanic plates in conjunction with the formation of new continental crust [23]. Upon examination of optAPM [30], the current state-of-the-art benchmark for plate motion modeling, it becomes apparent that the aforementioned datasets have not been implemented in a fashion that meets the standards of mathematical optimization. In this study, we approach this process from a more rigorous perspective in an effort to clarify errors and provide a more accurate prediction for the evolution of tectonic plate positions.

In 1912, Alfred Wegener first proposed the groundbreaking theory of continental drift [8], inspired by the matching coastlines of South America and Africa, suggesting the former existence of a supercontinent named Pangea that began to break apart around 200 million years ago (Ma). While initially met with skepticism, Wegener's theory gained widespread acceptance in the 1960s, following the discovery of tectonic plates—massive segments of Earth's lithosphere that glide over the flowing asthenosphere. This movement, driven by forces like mantle convection, slab pull, and ridge push, explain the gradual yet relentless drift of continents [28].

The emergence of plate motion models has allowed us to retrospectively map the positions of these plates to millions of years ago, offering invaluable insights into Earth's geological evolution at both local and global scales. The practical applications of plate tectonic modeling are ample. Notably, it allows for the prediction of seismic activity in earthquake-prone or volcanic areas, informing decisions in urban planning, infrastructure development, and disaster preparedness [10]. Additionally, such models have expanded our knowledge of other geological phenomena, especially at tectonic plate boundaries, including the development and dynamics of mountains and mid-ocean ridges [15, 14]. At a larger scale, they have contributed to our knowledge of supercontinent cycles [20], as well as our understanding of changes in seawater chemistry [32] and ore deposit distributions [6]. Overall, plate tectonic reconstructions are critical in geoscience disciplines like paleobiology, paleoclimate, geodynamics, and seismology.

In this paper, we investigate the leading absolute plate motion optimization procedure "optAPM," developed in [30]. The procedure refines these models using a comprehensive global inversion incorporating several key constraints: net lithospheric rotation, hotspot motion, and global trench migration. Each constraint is quantified by a cost function, and the process strives to minimize a unified objective function that encapsulates all three. In this project, we began with an analysis on the sensitivity of plate motion models. This was performed by observing the effects of introducing statistical "noise" to the rotation angle at model intervals. We then isolated individual constraints within the objective function, gauging the relative impact of each. This approach highlighted major discrepancies among the various outputs. After identifying pitfalls in the cost functions, we refined optAPM to address these concerns. Notably, we interpolated hotspot data and generated new data that aligns better with targeted reconstruction times. This streamlined the optimization process, allowing for a more direct calibration of the model output to the revised trail data. These procedural enhancements not only improved the model's accuracy but also fortified its statistical integrity, thus paving the way for a more objective and reliable understanding of plate movements.

This paper is structured as follows. In Section 1.1, we provide an introductory overview of plate motion models. In Section 2, we explore the various constraints used in optAPM, delineating the cost functions and clarifying the purposes of each. In Section 3, we examine the uncertainty inherent in plate motion models by introducing random variations to rotations and observing their propagation over time. In Section 4, we identify critical concerns in the optAPM code and present our own optimization methods, contrasting them with the original methods used. In Section 5, we assess the impact of our methods on model output, with a focus on the hotspot-dependent models. We also review how the three constraints converge into a single objective function, critiquing optAPM's approach at this.

1.1 Plate Motion Models

While recent technological advancements such as satellite geodesy have improved the accuracy and resolution of current tectonic plate measurements [2, 3], the reconstruction of historical plate positions is more complicated. Using data such as seafloor spreading records [13] and isochrons [21], scientists have been able to infer the relative motion of plates without directly observation.

Plate motion models exist primarily in two overarching categories, relative plate motion (RPM) models and absolute plate motion (APM) models. RPM models represent the dynamics of plate tectonics using a *reconstruction tree*, where nodes symbolize individual plates, identified by unique IDs, and edges define the interactions between neighboring plates. The foundational data of RPM models is incapsulated in a rotation model: a structured collection of tuples $(\alpha, \beta, \gamma, P, P_{ref}, t)$, where P and P_{ref} are denote the IDs of the tectonic plates, and the tuple (α, β, γ) signifies an Euler rotation that describes the position and orientation of plate P relative to the reference plate P_{ref} at a given time t million years ago. This hierarchical structure simplifies the task of deducing the relative motion between any pair of plates to a straightforward traversal of the tree's edges.

RPM models can model any portion of the Earth's surface [7, 27]. APM models generally build on existing RPM models by also establishing a relation between some assigned "root" plate and an absolute reference frame. In the case of optAPM specifically, the designated "root" plate is Africa, chosen for its centrality and connection to many major plates, with the mantle serving as the absolute reference frame. Alternatively, other models may use the Earth's spin axis as their absolute reference frame [19, 29].

2 Constraints in optAPM

In developing absolute plate motion (APM) models, researchers typically expand on a "global" relative plate motion (RPM) models, which encompass all the major tectonic plates

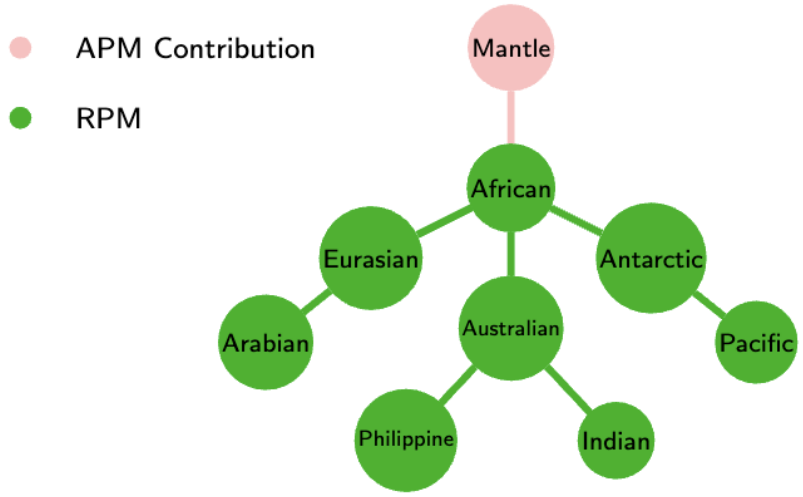

Figure 1: A schematic visualization of a reconstruction tree. Green nodes and edges represent information present in RPM models. The pink node and its corresponding edge represents the additional reference frame provided by the APM model, linking the African plate to the mantle.

and their interactions on Earth's surface. This foundational RPM model data is then utilized to fine-tune the absolute motion of an individual plate in relation to the mantle by optimizing some globally-dependent cost.

Most APM models adopt either the mantle or Earth's spin axis as their absolute reference frame. Models that utilize the spin axis draw on paleomagnetic data to determine the historical alignment of Earth's magnetic poles. APM that use the mantle as their reference frame, such as optAPM, are primarily informed by the analysis of hotspot trails. To minimize conflicts between disparate data sources, it is common practice in modeling studies to select a single constraint. However, beyond just hotspot trails, optAPM incorporates two other constraints, ensuring the model's geodynamic plausibility. This section will detail the purpose of the three constraints and the cost function associated with each.

2.1 Hotspot Trail Misfit

Hotspot trails form when tectonic plates slide over a mantle upwelling, leaving behind a traceable chain of volcanic formations on the seafloor. These mantle plumes, or hotspots, are considered stationary relative to the mantle for the purposes of plate reconstructions [16], due to their minimal velocities when compared to the faster-moving tectonic plates [25]. As such, when the present-day positions of hotspots are inverted back in time according to plate motion models, the resulting trajectories are expected to align closely with the empirical hotspot trail records. The code optAPM uses 9 well-documented hotspots spread across the globe: Cobb, Foundation, St. Helena, Tristan, Réunion, Tasmantid, Samoa,

Louisville, and Hawaii. These hotspots have all been studied extensively in prior research [25, 4, 11, 12, 17, 24, 35].

Distance between the predicted and observed hotspot location is computed using the great circle distance between two points on a globe, given by the formula

$$d = 2r \sin^{-1}\left(\sqrt{\left(\frac{\phi_2 - \phi_1}{2}\right) + \cos(\phi_1)\cos(\phi_2)\sin^2\left(\frac{\lambda_2 - \lambda_1}{2}\right)}\right),$$

where r is Earth's radius, ϕ_1 and ϕ_2 are the latitudes of the points, and λ_1 and λ_2 are the longitudes. Overall hotspot misfit is calculated with the cost function

$$HS_m = \sum_{i=0}^{n}(d_{1i} - d_{2i})^{-1} + HS_{gm}\sigma,$$

where d_{1i} is the predicted great circle distance between times T_i and T_{i-1}, d_{2i} is the observed great circle distance between times T_i and T_{i-1}, and $HS_{gm}\sigma$ is the global hotspot trail misfit standard deviation.

2.2 Global Trench Migration

In a self-consistent APM model, it is expected that subduction zone kinematics are plausible [26]. It has been shown that the following criteria are helpful for determining the plausibility of an APM model, both derived from past models and geodynamic modeling [5]:

- Maximize number of retreating trench segments and minimizing number of advancing trench segments,
- Minimize trench migration velocity at the center of wide subduction zones (due to the longer return flow path),
- Maximize number of retreating trench segments near edges of lateral slabs.

To compute trench migration in optAPM, plate boundaries are first extracted from the RPM model, and from these, global subduction zones are further extracted and sampled along the boundaries in 1° arc segments. At each iteration of the APM inversion, the absolute trench migration vectors orthogonal to each sampled segment are computed. Trench migration misfit is then calculated with the cost function

$$TM_k = \frac{\sum |V_T|}{T_n} + TM_{gT\sigma},$$

where TM_k is represents the misfit value corresponding to trench migration, $|V_T|$ is the

global trench-normal velocity vector, $TM_{gT\sigma}$ is the global trench-normal velocity standard deviation, and T_n is the total number of sampled trench segments.

2.3 Net Lithospheric Rotation

Lastly, the code also incorporates misfit relating to net lithospheric rotation. In past studies, geodynamic flow models provide the lowest estimates of NLR [1], while models incorporating hotspot data experienced the highest estimates of NLR [25, 31]. This procedure operates under the assumptions that lower rates of NLR are more likely, but NLR is not expected to equal zero. In particular, optAPM lower-bounds NLR to 0.08°/Myr and upper-bounds it to 0.20°/Myr, adding large costs for failing to meet these criteria. NLR magnitude is calculated with the cost function

$$\omega_{net} = 3/(8\pi r^4) \sum_i \int (\omega_i \times R) \times R dS_i,$$

where ω_{net} is the calculated NLR rate in degrees per million years, r is the radius of the Earth, R is the plate rotation velocity vector, dS is the area element integrated over the sphere, and ω is the plate angular velocity vector for a given plate.

2.4 Objective Function

For each iteration of the optimization process, the model optimizes absolute motion at some 5-million-year interval. In particular, it searches for the Euler rotation of Africa relative to the mantle which minimizes a cost determined by the objective function

$$J = \frac{HS_m}{\sigma_1} + \frac{TM_k}{\sigma_2} + \frac{\omega_{net}}{\sigma_3},$$

where σ_1, σ_2, and σ_3 are the relative weighings of each constraint. The determination of the Euler rotation involves the propagation of various Euler poles across the globe. At each of these poles, the model calculates the optimal rotation angle, effectively setting a "seed" for the iterative search that follows for a local minimum of the cost function. To enhance the model's resolution, additional seed poles can be introduced. A more detailed exposition of this optimization technique is detailed in Section 4.

However, the foundational paper on optAPM [30] omits a critical step in the transition from calculating individual cost functions to their union into a single objective function. Since these cost functions are not inherently comparable, the code introduces a scaling mechanism to normalize each constraint's influence on the optimal solution. Hence, the

objective function should be expressed as:

$$J = \frac{HS_m \cdot c_1}{\sigma_1} + \frac{TM_k \cdot c_2}{\sigma_2} + \frac{\omega_{net} \cdot c_3}{\sigma_3,}$$

where $c_1 = 0.125$, $c_2 = 1$, and $c_3 = 125$ are scaling constants applied to each constraint. The rationale behind such specific scaling values raises some concerns, which can potentially be addressed using a chi-square weighting instead.

3 Model Uncertainties

The task of constraining absolute plate motions is challenging, largely due to the discrete nature of geological data (both spatially and temporally), leading to many inaccuracies and uncertainties in the time-periods in between known data. In particular, the *world uncertainty*, or the percentage of the Earth's surface that has subducted since a given time, reaches as high as 60% by 140 million years ago (Ma) [31, 22]. As such, available hotspot data, predominantly existing on oceanic plates, also decreases significantly as we look further back in time. Methods for retrieving such subducted plates exist, such as the use of seismic tomography to locate large low-shear-velocity provinces [33]. Despite this, the data related to these geological anomalies remains imprecise, making direct reconstructions highly unreliable.

Moreover, the precise positions and velocities of present-day hotspots, key factors in plate motion models, are still highly debated in the scientific community [34]. Hotspots themselves are not entirely stationary relative to the mantle, and the velocity of rising mantle plumes is variable. Additionally, hotspots are disproportionately concentrated on the Pacific plate, introducing the risk of sampling bias and confounding factors. In the case of optAPM specifically, 4 out of the 9 hotspot trails used to constrain the data lie on the Pacific plate. To investigate potential discrepancies between hotspot trails, which deviate from each other at rates of up to 50 mm/yr, we generated models incorporating every subset of 7 hotspots of the 9 total hotspots. The resulting data can be found in Appendix 1.

Additionally, the vast amount of data informing a single plate motion model complicates the quantification of model uncertainty using standard metrics. Since model output relies on its preceding results, errors inherently compound and scale up as models date further back. To demonstrate this, we introduced controlled variability into the optimized plate motion model from [18]. Specifically, we perturbed the rotation angle of Laurentia relative to the mantle to be

$$\omega(1 + 0.1z),$$

where ω represents the original rotation angle, and z is a variable derived from a Gaussian

distribution centered at 0 with a standard deviation of 1. This process of error introduction was repeated across each 5-million-year interval, thereby simulating the accumulation of error back to 1000 Ma.

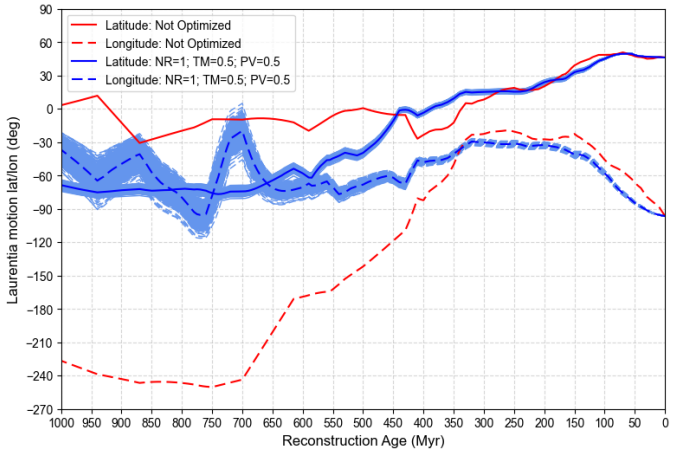

Figure 2: Reconstruction path of a reference point in Laurentia over the past 1000 million years, derived from models with introduced variability. The intermediate rotation angle ω is adjusted at 5 Myr intervals using the function $\omega(1 + 0.1z)$, where z is a random variable derived from a Gaussian distribution centered at 0 with standard deviation 1. The red lines depict the latitudinal and longitudinal paths from the unoptimized model, while the dark blue lines show the same for the optimized model. The shaded blue areas represent the variability among 1000 perturbed model. Solid lines indicate latitude and dashed lines indicate longitude.

Figure 2 illustrates the variations in Laurentia's latitudinal and longitudinal movements over 1000 simulations. The unoptimized rotation model's trajectories are depicted by the red lines, while the optimized model's trajectories are represented by the dark blue lines. As expected, Laurentia experiences lower rates of rotation in the optimized model. The paler blue shaded areas surrounding the optimized paths indicate the range of plate motions across the 1000 perturbed models. Notably, at 1000 Ma, the spread of possible positions for Laurentia spans approximately 35 degrees in latitude and about 10 degrees in longitude.

4 Methods and Model Setup

For our reconstructions, we adapted the publicly available optAPM code, implementing substantial enhancements to both the optimization process and the cost function definitions. Our chosen relative plate motion model from [18] offers a comprehensive global reconstruction dating back to 1000 Ma. In addition to describing relative motion between plates, this model captures topological changes over time, providing a nuanced picture of net lithospheric rotation and enabling more precise calculations.

Our code optimized absolute plate motion at 5-million-year increments. However, our reconstructions were limited to the past 80 million years, reflecting the consensus that hotspot data beyond this point lacks sufficient reliability. At each interval, the code computed the Euler rotation of the African plate relative to the mantle which minimizes the objective function, and updated the APM model accordingly. A detailed visual representation of this modeling process is available in the flowchart depicted in Figure 3.

To identify local minima from seed poles, our method utilized the COBYLA algorithm (short for Constrained Optimization BY Linear Approximations) as integrated within the NLopt optimization library [9]. For each interval, our method propagated a collection of 105 "seed" Euler rotations, uniformly distributed within a 60° radius of the preceding optimal Euler pole. Beginning from each of these estimates, COBYLA systematically searched for a local minimum objective function value, and our method then extracted a global minimum from the local minima. COBYLA is particularly effective in complex, constraint-rich environments and operates independently of gradient information. While we typically allowed COBYLA to reach full convergence to a local minimum, we imposed a cap of 1000 iterations on runs that were especially computationally demanding, such as those involving isolated trench migration, to prevent infinite convergence cycles.

4.1 Isolating Constraints

To enhance the optimization procedure's robustness, we conducted an examination of the models resulting from the isolation of individual constraints within the code. In the context of the objective function

$$J = \frac{HS_m}{\sigma_1} + \frac{TM_k}{\sigma_2} + \frac{\omega_{net}}{\sigma_3},$$

we set two of the variables, σ_1, σ_2, and σ_3, to infinity, while fixing the third at 1. For the cost functions of net lithospheric rotation and global trench migration, we eliminated the lower bounds, recognizing that they hold little relevance in the absence of accompanying constraints. After implementing these changes, we executed the optimization procedure three times, generating a model corresponding to each constraint.

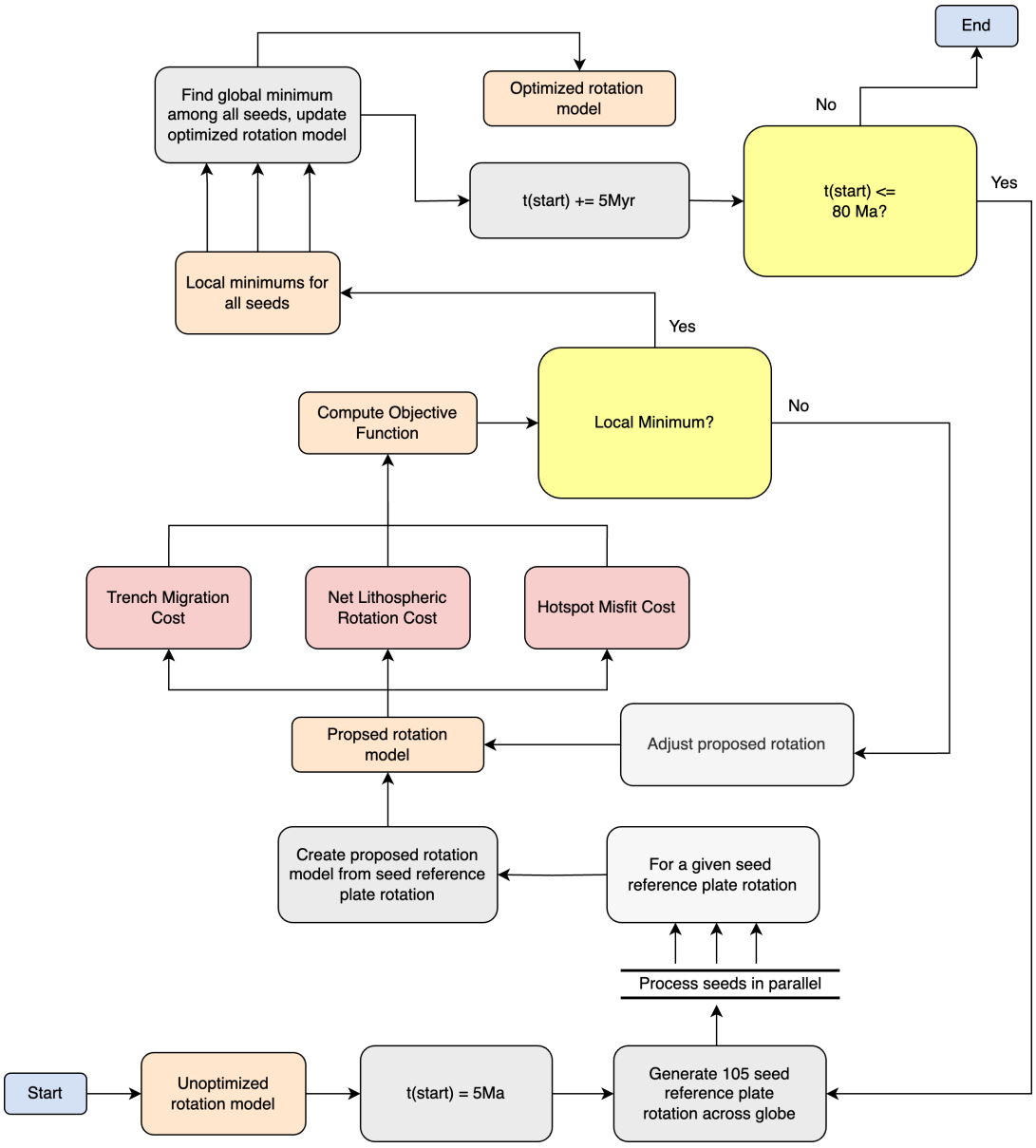

Figure 3: Workflow diagram illustrating the full optimization process. The code optimizes absolute plate motion at 5-million-year (5Myr) intervals, dating back to 80 Ma. The African plate is used as the reference throughout the procedure, chosen for its central position and close relationship with other major plates. At each interval, the code propagates a collection of 105 "seed" Euler rotations, uniformly distributed within a 60° radius of the preceding optimal Euler pole. For each seed rotation, the algorithm creates a temporary rotation model. This model is then used to calculate the value of the objective function, guiding the algorithm through iterative adjustments toward a local minimum. The process then determines a global minimum from these local minima, incrementally refining the plate motion model.

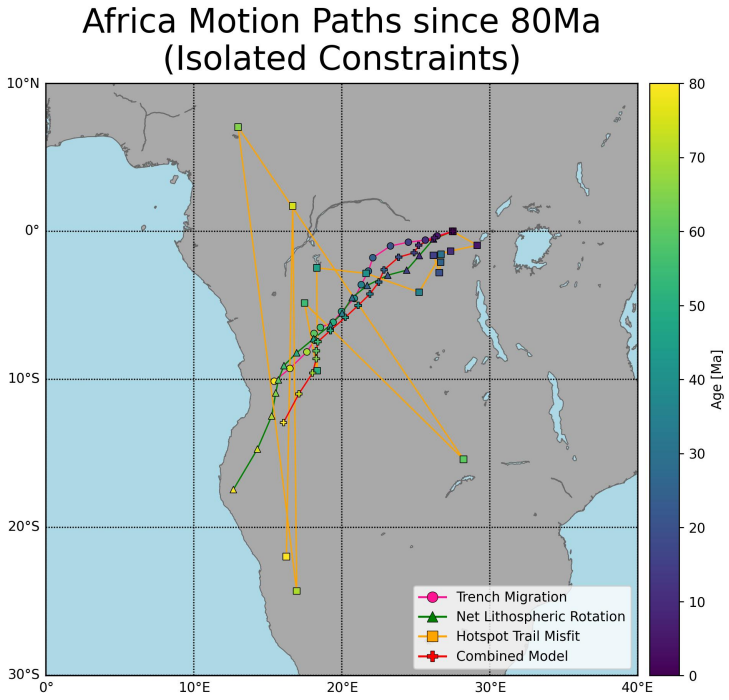

Figure 4: Predicted motion paths when the point at (0°N, 27.5°E) in the African plate is reconstructed back to 80 Ma according to three different models, each isolating a different model constraint: trench migration (pink circles), net lithospheric rotation (green triangles), and hotspot trail misfit (orange squares). Additionally, the red plus signs indicate the integrated model that considers all three constraints simultaneously. The models operate on 5 Myr intervals, with varying colors denoting the age of the reconstructed position.

Figure 4 depicts the resulting motion paths when we used each of the three models, as well as a model combining all three, to reconstruct a point (0°N, 27.5°E) in the African plate. The results drew attention to significant issues with the hotspot cost function, which become apparent when this function was singled out during optimization. Specifically, the hotspot-only model predicted an average velocity of 22.1 cm/yr, in contrast to the average velocities of 2.8 cm/yr and 2.2 cm/yr from the models isolating trench migration and net lithospheric rotation, respectively. We address these discrepancies in the following subsection.

4.2 Changes to Cost Functions

Our initial refinement of the optAPM model addressed the cost functions associated with hotspot data and trench migration. The original cost functions employed standard deviation as a measure for these constraints, a choice that was not sufficiently justified within the existing documentation. To achieve a more straightforward and transparent set of criteria, we opted to utilize the average for both constraints. However, the primary underlying issue pertained to other aspects of the hotspot cost function.

The original hotspot cost function followed a few main steps:

1. Create proposed rotation model at reconstruction time.
2. Search for all hotspot trail data within a 10Myr interval succeeding the reconstruction time.
3. For all hotspot data points, at the *hotspot data time*, compute distance between:
    - Raw hotspot trail data, and
    - **Interpolated** model output.
4. Minimize distance median + standard deviation.

We implemented a new hotspot cost function with the following steps:

1. Create proposed rotation model at reconstruction time.
2. Interpolate all hotspot data to reconstruction time.
3. For all hotspot trails, at the *reconstruction time*, compute distance between:
    - **Interpolated** hotspot trail data, and
    - Raw model output at reconstructed time.
4. Minimize distance average.

Fundamentally, the previous model sought to optimize the interpolation points interspersed among the model's outputs, while our updated model focuses directly on optimizing the model outputs themselves, effectively mitigating the accumulation of errors over time. Figure 5 illustrates an outlier case in which all hotspot trail data falls precisely between multiple of 5 Myrs. By streamlining the model to consider only a single hotspot trail, it becomes clear that the revised model, adhering to the new cost function, maintains a trajectory that is much more consistent with the hotspot trail data, unlike the previous model which fluctuated significantly around the trail data.

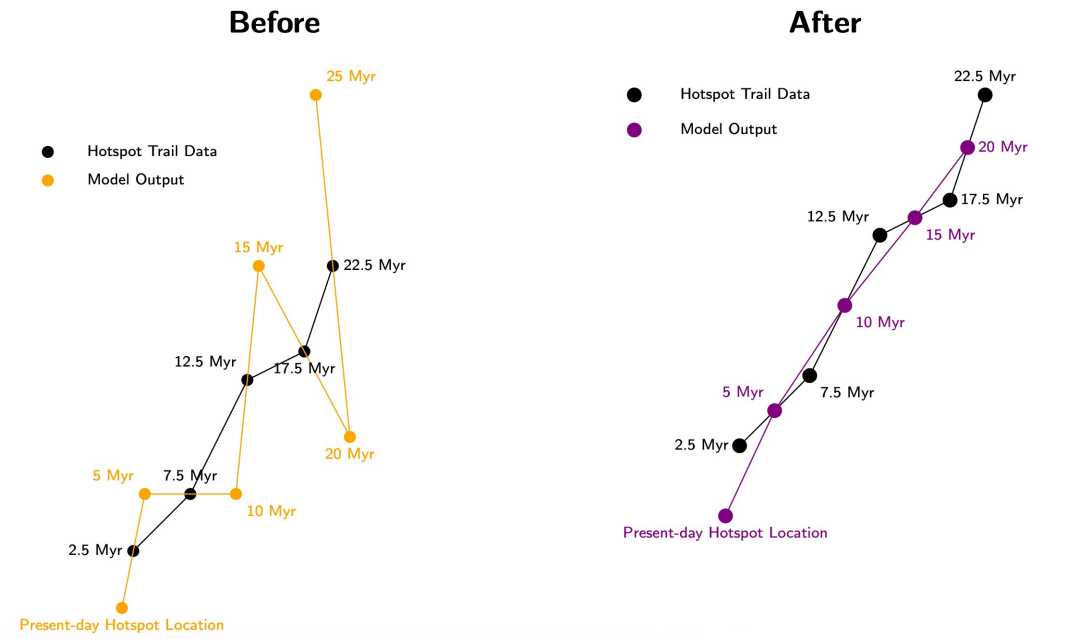

Figure 5: A comparative illustration of model performance before and after the implementation of the new hotspot cost function, focusing on a single hotspot trail for clarity. The black lines represent the actual hotspot trail data. On the left (Before), the orange trajectory shows the model output using the original cost function, which minimizes distances at times corresponding to raw hotspot trail data. On the right (After), the purple trajectory depicts the model output using the revised cost function, which minimizes distances precisely at the reconstruction times. In this special case, the model output of the revised hotspot cost function perfectly matches the interpolated hotspot trail data.

5 Results and Analysis

Following our new hotspot cost function, we began by interpolating all hotspot data to integral 5-million-year increments. After performing this interpolation, we derived a new model, once again isolating the hotspot constraint. To assess the impact of our modifications, we reintegrated the three cost functions and generated a revised comprehensive model. Finally, we conducted a comparative analysis between this new, comprehensive model and its predecessor, which now included the refined hotspot cost function. All models range from 80-0Ma. As in Figure 4, we reconstruct the point (0°N, 27.5°E) in our diagrams.

Since tectonic plates typically traverse linear paths and hotspots are approximately fixed in relation to the mantle, the resulting hotspot data exhibited a relative smoothness. Hence, the interpolated trails yielded trajectories that remain consistent with the raw hotspot trails, as depicted in Figure 6. Individual hotspot data points, however, underwent significant adjustments due to temporal inconsistencies in the data and the mechanics of the interpolation

process itself.

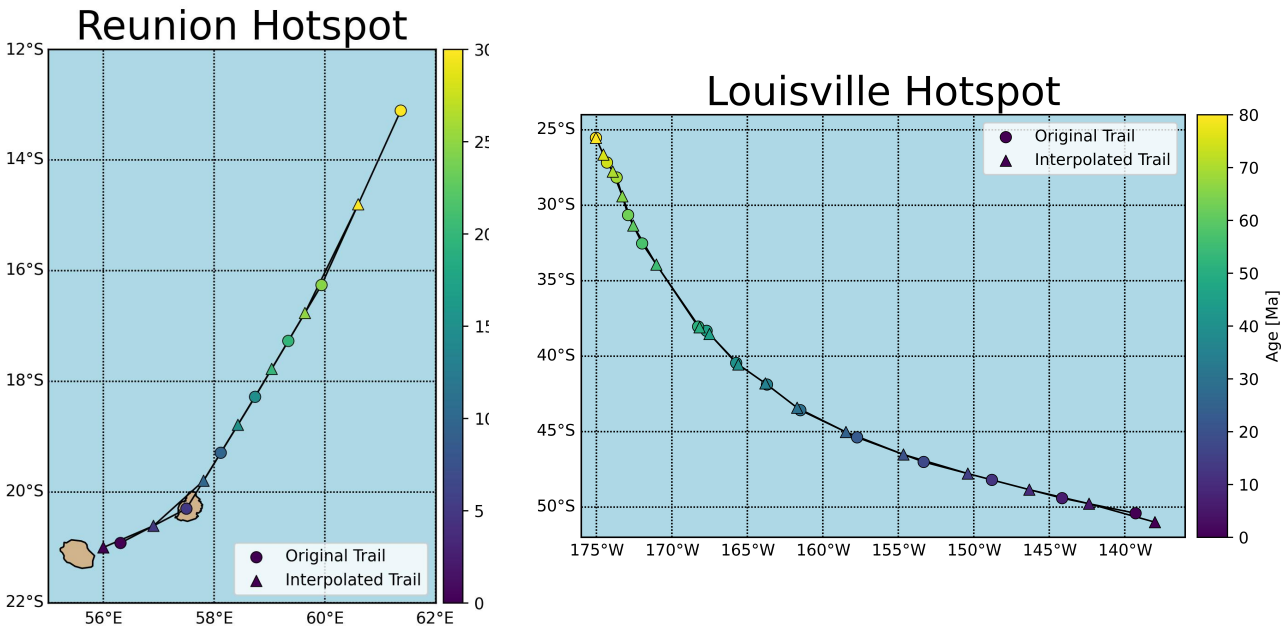

Figure 6: A comparison between raw hotspot trail data and interpolated hotspot trail data in two well-studied hotspots, Reunion and Louisville. Circles represent the raw hotspot trail data and triangles represent the interpolated hotspot trail data. Color represents age in Ma.

While changes in hotspot trail data were minimal, the effects on model output were instrumental. Figure 7 extends the analysis presented in Figure 4 by incorporating the model generated by isolating the newly implemented hotspot cost function. These changes reflect the trends shown in Figure 5, where the updated model demonstrates a more consistent and linear progression compared to its predecessor. The previous model estimated the African plate's average absolute velocity to be about 22.1 cm/year, with an average angular variation of roughly 57.5 degrees over 5-million-year periods. In contrast, the revised model reported a significantly reduced average plate velocity of approximately 2.6 cm/year and an angular variation of just 17.0 degrees, illustrating a substantial improvement in the model's consistency.

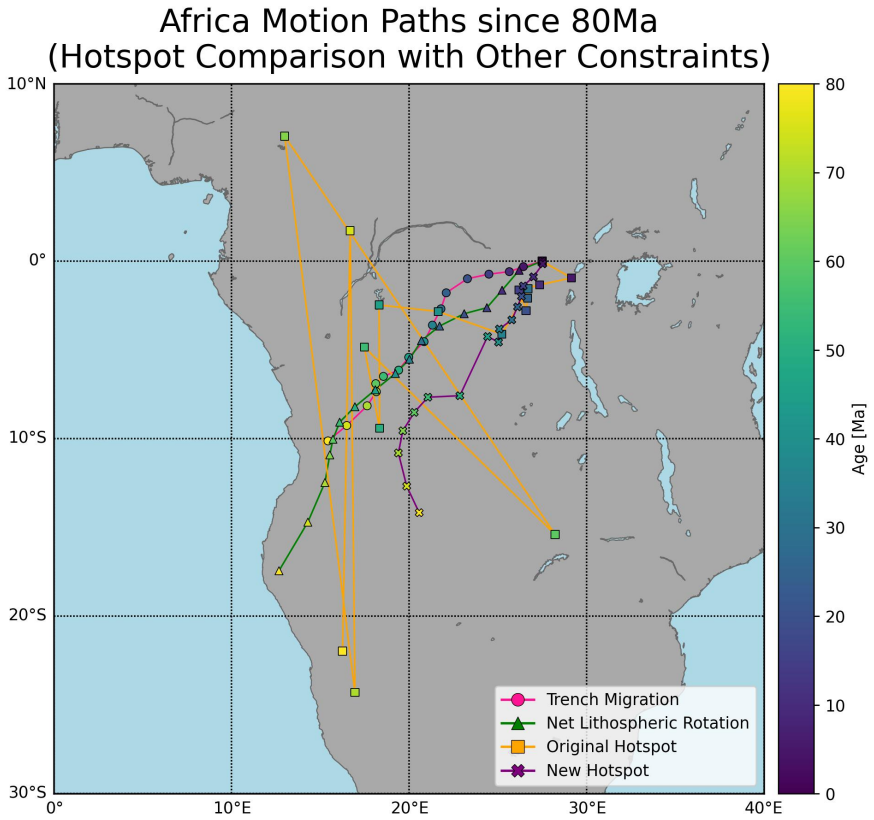

Figure 7: Same data-generation process as Figure 4. Purple "X" symbols correspond to the model isolating the revised hotspot trail mistfit cost function.

Furthermore, the refined hotspot-only model exhibited a significantly improved alignment with additional geological constraints, as seen in Figure 8. The new model predicted an average trench migration velocity of just 0.87 cm/year, which was a substantial reduction from the previously estimated 5.42 cm/year. Moreover, all median trench migration values were positive and less than 2 cm/year, aligning with geodynamic models that suggest a low but positive rate of trench migration. The standard deviation for trench migration in the updated model was also significantly reduced to 0.40 cm/year, in contrast to the earlier 8.23 cm/year, indicating a more stable and consistent modeling outcome.

In terms of net lithospheric rotation (NLR), the new model presented a rate of 0.26°/Myr, much lower than the 2.78°/Myr calculated by the original model. This rate is in agreement with historical hotspot-based models, which typically yield NLR values between 0.10 and 0.50°/Myr. Nonetheless, it is noted that the modeled NLR still slightly surpasses the geodynamic predictions, which range from 0.05 to 0.15°/Myr.

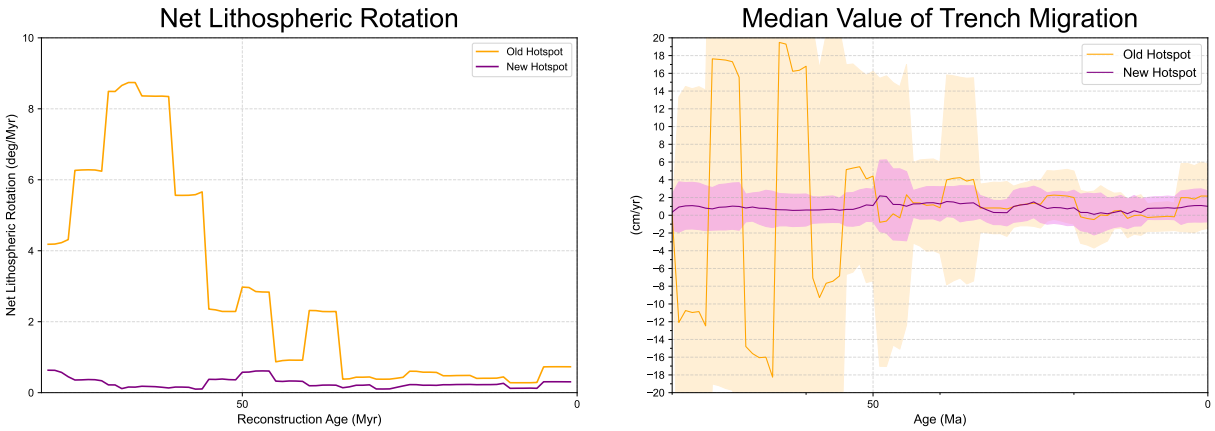

Figure 8: A comparison of the net lithospheric rotation and median trench migration as predicted by the old and new hotspot models. Orange lines represent outcomes from the model using the original hotspot cost function, while the purple lines denote results from the model using the updated cost function. The shaded regions around around median trench migration indicate the range of trench migration velocities at given times.

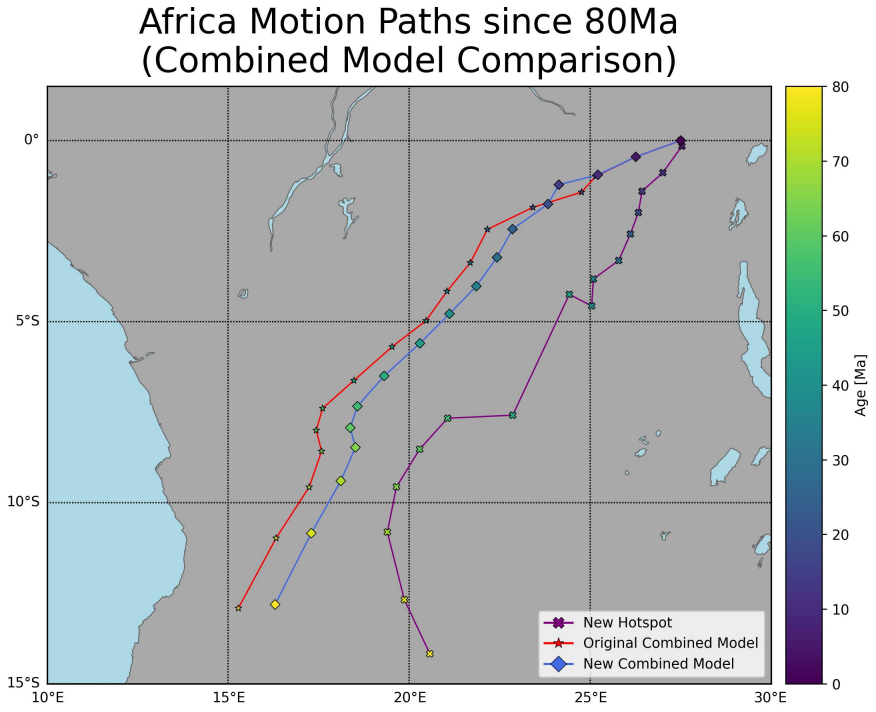

Figure 9: Same data-generation process as Figure 4. Purple "X" symbols correspond to the model isolating the revised hotspot trail mistfit cost function. Red stars represent the original comprehensive model, and blue diamonds represent the updated comprehensive model, which utilizes the revised cost functions.

Figure 9 illustrates the effectiveness of the revised hotspot cost function within a comprehensive plate motion model that integrated all three constraints. The model incorporating the new cost function, indicated by blue diamonds, showed a reduced average deviation of 315.21 km from the expected path: a notable improvement over the original model's deviation of 378.73 km, denoted by red stars. This suggests a refinement in the model's ability to predict and minimize errors across various hotspot tracks, likely due to the more streamlined optimization process.

Acknowledgements

This work was completed as part of the MIT PRIMES program.

Appendix 1:

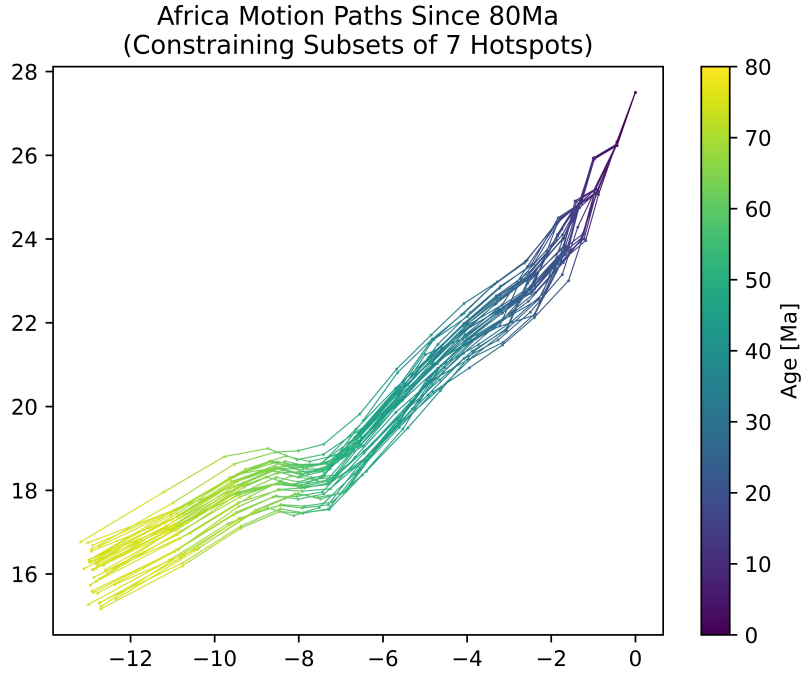

Figure 10: Predicted motion paths when the point (0°N, 27.5°E) in the African plate is reconstructed back to 80 Ma for 36 different models, each incorporating a unique subset of 7 hotspots from the 9 total hotspots utilized in optAPM. Color represents age in millions of years, and individual line segments between adjacent points represent absolute motion in a 5 Myr interval period.

Figure 10 illustrates the reconstructed motion paths derived from 36 distinct models, each constrained by a unique subset of 7 out of the 9 total hotspots employed by optAPM. The incremental progressions of these paths are largely consistent across the different models,

a similarity attributed to the governing constraints of net lithospheric rotation (NLR) and trench migration (TM). Nevertheless, there is a noticeable divergence among the models, with a dispersion of up to approximately 3° in longitude, which can be traced back to variations in hotspot trail data. This divergence underscores the role of hotspots in fine-tuning the model outputs, while also emphasizing that the overarching trajectory is shaped by NLR and TM constraints.

References

[1] Thorsten W Becker. Superweak asthenosphere in light of upper mantle seismic anisotropy. *Geochemistry, Geophysics, Geosystems*, 18(5):1986–2003, 2017.

[2] Charles DeMets, Richard G Gordon, and Donald F Argus. Geologically current plate motions. *Geophysical journal international*, 181(1):1–80, 2010.

[3] Charles DeMets, Richard G Gordon, Donald F Argus, and Seth Stein. Current plate motions. *Geophysical journal international*, 101(2):425–478, 1990.

[4] Pavel V Doubrovine, Bernhard Steinberger, and Trond H Torsvik. Absolute plate motions in a reference frame defined by moving hot spots in the pacific, atlantic, and indian oceans. *Journal of Geophysical Research: Solid Earth*, 117(B9), 2012.

[5] Nicolas Flament, Simon Williams, RD Müller, Michael Gurnis, and Dan J Bower. Origin and evolution of the deep thermochemical structure beneath eurasia. *Nature communications*, 8(1):14164, 2017.

[6] Donald Forsyth and Seiya Uyeda. On the relative importance of the driving forces of plate motion. *Geophysical Journal International*, 43(1):163–200, 1975.

[7] Michael Gurnis, Mark Turner, Sabin Zahirovic, Lydia DiCaprio, Sonja Spasojevic, R Dietmar Müller, James Boyden, Maria Seton, Vlad Constantin Manea, and Dan J Bower. Plate tectonic reconstructions with continuously closing plates. *Computers & Geosciences*, 38(1):35–42, 2012.

[8] Anthony Hallam. Alfred wegener and the hypothesis of continental drift. *Scientific American*, 232(2):88–97, 1975.

[9] Steven G Johnson and Julien Schueller. Nlopt: Nonlinear optimization library. *Astrophysics Source Code Library*, pages ascl–2111, 2021.

[10] T Jordan, Y-T Chen, Paolo Gasparini, Raul Madariaga, Ian Main, Warner Marzocchi, Gerassimos Papadopoulos, K Yamaoka, J Zschau, et al. Operational earthquake forecasting: State of knowledge and guidelines for implementation. *Annals of Geophysics*, 2011.

[11] Kurt M Knesel, Benjamin E Cohen, Paulo M Vasconcelos, and David S Thiede. Rapid change in drift of the australian plate records collision with ontong java plateau. *Nature*, 454(7205):754–757, 2008.

[12] Anthony AP Koppers, Molly D Gowen, Lauren E Colwell, Jeffrey S Gee, Peter F Lonsdale, John J Mahoney, and Robert A Duncan. New 40ar/39ar age progression for the louisville hot spot trail and implications for inter–hot spot motion. *Geochemistry, Geophysics, Geosystems*, 12(12), 2011.

[13] TM Kusky, BF Windley, I Safonova, K Wakita, J Wakabayashi, A Polat, and M Santosh. Recognition of ocean plate stratigraphy in accretionary orogens through earth history: A record of 3.8 billion years of sea floor spreading, subduction, and accretion. *Gondwana Research*, 24(2):501–547, 2013.

[14] Jian Lin and EM Parmentier. Mechanisms of lithospheric extension at mid-ocean ridges. *Geophysical Journal International*, 96(1):1–22, 1989.

[15] Ken C Macdonald. Mid-ocean ridges: Fine scale tectonic, volcanic and hydrothermal processes within the plate boundary zone. *Annual Review of Earth and Planetary Sciences*, 10(1):155–190, 1982.

[16] SM Maher, P Wessel, RD Müller, SE Williams, and Y Harada. Absolute plate motion of africa around hawaii-emperor bend time. *Geophysical Journal International*, 201(3):1743–1764, 2015.

[17] Ian McDougall and Robert A Duncan. Age progressive volcanism in the tasmantid seamounts. *Earth and Planetary Science Letters*, 89(2):207–220, 1988.

[18] Andrew S Merdith, Alan S Collins, Simon E Williams, Sergei Pisarevsky, John D Foden, Donnelly B Archibald, Morgan L Blades, Brandon L Alessio, Sheree Armistead, Diana Plavsa, et al. A full-plate global reconstruction of the neoproterozoic. *Gondwana Research*, 50:84–134, 2017.

[19] Ross N Mitchell, Taylor M Kilian, and David AD Evans. Supercontinent cycles and the calculation of absolute palaeolongitude in deep time. *Nature*, 482(7384):208–211, 2012.

[20] R Dietmar Müller, Nicolas Flament, John Cannon, Michael G Tetley, Simon E Williams, Xianzhi Cao, Ömer F Bodur, Sabin Zahirovic, and Andrew Merdith. A tectonic-rules-based mantle reference frame since 1 billion years ago–implications for supercontinent cycles and plate–mantle system evolution. *Solid Earth*, 13(7):1127–1159, 2022.

[21] R Dietmar Müller, Walter R Roest, Jean-Yves Royer, Lisa M Gahagan, and John G Sclater. Digital isochrons of the world's ocean floor. *Journal of Geophysical Research: Solid Earth*, 102(B2):3211–3214, 1997.

[22] R Dietmar Müller, Maria Seton, Sabin Zahirovic, Simon E Williams, Kara J Matthews, Nicky M Wright, Grace E Shephard, Kayla T Maloney, Nicholas Barnett-Moore, Maral Hosseinpour, et al. Ocean basin evolution and global-scale plate reorganization events since pangea breakup. *Annual Review of Earth and Planetary Sciences*, 44:107–138, 2016.

[23] Rajeev Nair and Thomas Chacko. Role of oceanic plateaus in the initiation of subduction and origin of continental crust. *Geology*, 36(7):583–586, 2008.

[24] John M O'Connor, Bernhard Steinberger, Marcel Regelous, Anthony AP Koppers, Jan R Wijbrans, Karsten M Haase, Peter Stoffers, Wilfried Jokat, and Dieter Garbe-Schönberg. Constraints on past plate and mantle motion from new ages for the hawaiian-emperor seamount chain. *Geochemistry, Geophysics, Geosystems*, 14(10):4564–4584, 2013.

[25] Craig O'Neill, Dietmar Müller, and Bernhard Steinberger. On the uncertainties in hot spot reconstructions and the significance of moving hot spot reference frames. *Geochemistry, Geophysics, Geosystems*, 6(4), 2005.

[26] W.P. Schellart, D.R. Stegman, and J. Freeman. Global trench migration velocities and slab migration induced upper mantle volume fluxes: Constraints to find an earth reference frame based on minimizing viscous dissipation. *Earth-Science Reviews*, 88(1):118–144, 2008.

[27] Müller Seton, R Dietmar Müller, S Zahirovic, C Gaina, T Torsvik, G Shephard, A Talsma, M Gurnis, M Turner, S Maus, et al. Global continental and ocean basin reconstructions since 200 ma. *Earth-Science Reviews*, 113(3-4):212–270, 2012.

[28] Richard H Sillitoe. A plate tectonic model for the origin of porphyry copper deposits. *Economic geology*, 67(2):184–197, 1972.

[29] Bernhard Steinberger and Trond H Torsvik. Absolute plate motions and true polar wander in the absence of hotspot tracks. *Nature*, 452(7187):620–623, 2008.

[30] Michael G Tetley, Simon E Williams, Michael Gurnis, Nicolas Flament, and R Dietmar Müller. Constraining absolute plate motions since the triassic. *Journal of Geophysical Research: Solid Earth*, 124(7):7231–7258, 2019.

[31] Trond H Torsvik, Bernhard Steinberger, Michael Gurnis, and Carmen Gaina. Plate tectonics and net lithosphere rotation over the past 150 my. *Earth and Planetary Science Letters*, 291(1-4):106–112, 2010.

[32] Alexandra V Turchyn and Donald J DePaolo. Seawater chemistry through phanerozoic time. *Annual Review of Earth and Planetary Sciences*, 47:197–224, 2019.

[33] Douwe G Van Der Meer, Wim Spakman, Douwe JJ Van Hinsbergen, Maisha L Amaru, and Trond H Torsvik. Towards absolute plate motions constrained by lower-mantle slab remnants. *Nature Geoscience*, 3(1):36–40, 2010.

[34] Chengzu Wang, Richard G Gordon, and Tuo Zhang. Bounds on geologically current rates of motion of groups of hot spots. *Geophysical Research Letters*, 44(12):6048–6056, 2017.

[35] Paul Wessel and Loren W Kroenke. The geometric relationship between hot spots and seamounts: Implications for pacific hot spots. *Earth and Planetary Science Letters*, 158(1-2):1–18, 1998.